Available online at www.sciencedirect.com

SciVerse ScienceDirect

Ceramics International 39 (2013) 7627–7634

CERAMICS INTERNATIONAL

www.elsevier.com/locate/ceramint

Microstructure and anisotropic mechanical properties of graphene nanoplatelet toughened biphasic calcium phosphate composite

Yan Zhao[a,b], Kang-Ning Sun[a,b,*], Wei-Li Wang[a,b], Yu-Xiang Wang[a,b], Xiao-Lin Sun[a,b], Yan-Jie Liang[a,b], Xiao-Ning Sun[a,b], Peng-Fei Chui[a,b]

[a]*Key Laboratory for Liquid–Solid Structural Evolution and Processing of Materials, Ministry of Education, Shandong University, Jinan 250061, PR China*

[b]*Engineering Ceramics Key Laboratory of Shandong Province, Shandong University, Jinan 250061, PR China*

Received 22 February 2013; accepted 5 March 2013
Available online 14 March 2013

Abstract

Graphene nanoplatelets (GNPs) reinforced biphasic calcium phosphate (BCP) composites were prepared by hot pressing (HP). Based on in-depth mechanical test and observation of microstructure, the influence of GNPs on BCP matrix was investigated. A preferred orientation of GNPs occurred during sintering, leading to anisotropic mechanical properties. The mechanical properties of GNPs/BCP composite measured along the direction parallel to the HP direction are higher than those measured along the perpendicular direction. Parallel to the HP direction, the composite containing 1.5 wt% GNPs exhibited the maximun bending strength and fracture toughness of 151.82 MPa and 1.74 MPa $m^{1/2}$, about 55% and 76% higher than those of monolithic BCP, respectively. The improvement in mechanical properties was mainly attributable to crack deflection, crack branching, bridging, pullout and fracture of GNPs. Especially GNPs can force crack to propagate not only in two but also in three dimensions.

Keywords: A. Hot pressing; B. Composites; C. Mechanical properties; D. Apatite

1. Introduction

Graphene with two-dimensional high aspect ratio layer geometry and large specific surface area is predicted to have a range of unusual properties [1,2]. Both theoretical and experimental studies have proved that graphene has extraordinary mechanical properties: Young's modulus is up to 1 TPa and intrinsic strength is approximately 130 GPa [3–5]. Besides, graphene possesses outstanding electronic and thermal properties, such as high carrier mobility at room temperature (10,000–20,000 $cm^2\ V^{-1}\ s^{-1}$) and excellent thermal conductivity (3000–5000 $W\ m^{-1}\ K^{-1}$) [6,7]. These great properties make it a promising candidate for practical applications in sensing, catalysis, electronics, energy storage and conversion, etc. [8]. Especially, these theoretical and experimental values indicate that graphene can be used as an excellent reinforcing/functionalizing element for ceramic materials [9].

Being one of the most promising reinforcing agent, graphene has also been used to increase the mechanical performance of ceramics, such as Al_2O_3 [10], ZTA [11], Si_3N_4 [12–15], and hydroxyapatite (HA) [16]. For all the composites, fracture toughness was significantly improved in comparison to the monolithic, in which the main toughening mechanisms were crack deflection, crack branching and crack bridging.

As well as mechanical properties, greatly improved conductivity was observed in experiments of Fan and Wang, in which graphene nanosheet/Al_2O_3 composites were prepared by spark plasma sintering (SPS) [10,17]. In particular, Ramirez et al. and

Abbreviations: HA, hydroxyapatite; SPS, spark plasma sintering; GNPs, graphene nanoplatelets; BCP, biphasic calcium phosphate; β-TCP, beta-tricalcium phosphate; CDA, calcium-deficient apatite; CTAB, cetyltrimethylammonium bromide; HP, hot pressing

*Corresponding author at: Key Laboratory for Liquid–Solid Structural Evolution and Processing of Materials, Ministry of Education, Shandong University, Jinan 250061, PR China. Tel./fax: +86 531 88392914.
E-mail address: sunkangning@sdu.edu.cn (K.-N. Sun).

0272-8842/$ - see front matter © 2013 Elsevier Ltd and Techna Group S.r.l. All rights reserved.
http://dx.doi.org/10.1016/j.ceramint.2013.03.018

Miranzo et al. fabricated graphene nanoplatelets (GNPs)/Si_3N_4 composites, and found anisotropic electrical conductivity and thermal conductivity in the samples [18–20]. During compaction and pressure-assisted densification, a preferred orientation of GNPs occurred in the matrix. The electrical conductivity measured along the direction perpendicular to the SPS pressing axis is more than one order of magnitude higher than the one measured along the parallel direction. However, there is no report about anisotropic mechanical properties yet.

Biphasic calcium phosphate (BCP) is a mixture which consists of HA, $Ca_{10}(PO_4)_6(OH)_2$, and beta-tricalcium phosphate (β-TCP), β-$Ca_3(PO_4)_2$, and of varying HA/β-TCP ratio. It can be obtained through calcining of calcium-deficient apatite (CDA) at high temperature or mechanical mixing of HA and β-TCP. Due to its excellent biocompatibility and osteoconductivity of HA and degradability of β-TCP, BCP is an attractive ceramic material for bone substitution and reconstruction. However, lack of sufficient strength and toughness limits its applications in under-load conditions [21–23].

In the present work, GNPs were introduced into BCP bioceramic to enhance the mechanical properties. The GNPs/BCP composites were investigated in detail with respect to phase compositions, microstructures, and anisotropic mechanical properties. Based on careful characterization and test, toughening mechanisms were discussed.

2. Experimental

GNPs, approximately 0.5–20 μm in length and width and 1–5 nm in thickness, were used as the toughening agent. They were provided by Nanjing XFNANO Materials Tech Co., Ltd. For BCP, first, CDA nanopowders were prepared by chemical precipitation of $Ca(NO_3)_2$ and $(NH_4)_2HPO_4$ with an appropriate Ca/P ratio. Then, BCP nanpowders, a mixture of 70 wt% HA and 30 wt% β-TCP were collected after calcining the obtained CDA at 550 °C.

GNPs were dispersed in cetyltrimethylammonium bromide (CTAB) solution by sonication for 1 h. Then the suspension and BCP nanopowders were mixed by ball milling for 8 h. After being dried, such mixtures were treated at 500 °C for 1 h in argon to remove the surfactant. Finally, the composites were fabricated by hot pressing (HP) the screened powders at 1150 °C in a multipurpose hightemperature furnace (Fujidenpa Kogyo Co., Ltd., Osaka, Japan) under a pressure of 30 MPa in an argon atmosphere for 1 h. The contents of GNPs in the composites were 0, 0.5, 1.0, 1.5, 2.0 and 2.5 wt%.

The mixture powders as well as polished and fracture surfaces of bulk samples were characterized by field-emission scanning electron microscopy (FESEM, SU-70, Hitachi, Japan). The phases were determined by X-ray diffraction (XRD, Rigaku DMAX-2500PC, Japan) using Cu Kα radiation, and the interface between GNPs and matrix was characterized by a high resolution transmission electron microscope (HRTEM, Tecnai 20U-TWIN, Philips, Holand). Besides, all the samples were polished and thermally etched at 1050 °C for 30 min in a muffle furnace for grain size determination. Image analysis software was applied to determine the average grain size, using 150–200 grains for each sample. The densities were determined by the Archimedes method with distilled water as the immersion medium, and theoretical densities of 3.16, 3.07 and 2.25 g/cm^3 were adopted for HA, β-TCP and GNPs, respectively.

Bending strength, fracture toughness and microhardness were measured along two directions: parallel and perpendicular to the HP direction. The sintered samples were machined into rectangular specimens 3.0 mm × 4.0 mm × 25.0 mm in size for bending strength and fracture toughness measurements. Each specimen was ground, and the edges were polished in order to reduce stress concentration. Furthermore, a notch of 2.0 mm depth was cut using a thin diamond blade in the middle of each specimen for fracture toughness test. Bending strength was measured by three-point bending test at a speed of 0.5 mm/min, and fracture toughness was measured by the single-edge notched beam (SENB) method at a speed of 0.05 mm/min. Both tests were conducted on a CMT5101 electromechanical universal testing mechine (Shenzhen SANS Testing Machine Co., Ltd.) with a span length of 20.0 mm at room temperature. The resulting values were the average of four or five specimens for each. Microhardness was measured using a microhardness tester (HX-1000, Shanghai) with Vickers probe applying 500 g of load for 15 s of dwell time on a polished surface. Ten indentations on the randomly selected area of each sample were performed at room temperature.

3. Results and discussion

3.1. Mixture powders

The pristine GNPs and 1.5 wt% GNPs/BCP composite powders were examined by FESEM. Fig. 1a shows the morphology of the pristine GNPs, whose length and width extend up to several micrometers and thickness less than several nanometers. Fig. 1b displays the dispersion of GNPs. GNPs, which are coated with BCP particles, are uniform in the mixture with no damage, and the size of BCP particles is approximately 50 nm. Due to the powder shell, the plate like structure becomes thicker.

Graphene is easy to agglometate because of its two-dimensional high aspect ratio sheet geometry and the layer interaction [24]. The mechanical properties of composites depend on the dispersion of GNPs in the matrix. HA and β-TCP usually have negative charge due to the deficiency of calcium ions. In this experiment, cationic surfactant CTAB was employed as the dispersant to make GNPs surface with positive charge. The BCP nanopowders can be attracted to the GNPs surface owing to electrostatic interaction once GNPs suspension was mixed with them, thereby preventing GNPs from agglomerating.

3.2. Phase composition analysis

XRD patterns of GNPs/BCP composites are presented in Fig. 2. The peaks in all six patterns are indexed as HA (JCPDS no. 74-0566) and β-TCP (JCPDS no. 70-2065). All the peaks are sharp and the intensities are high, indicating that the grains

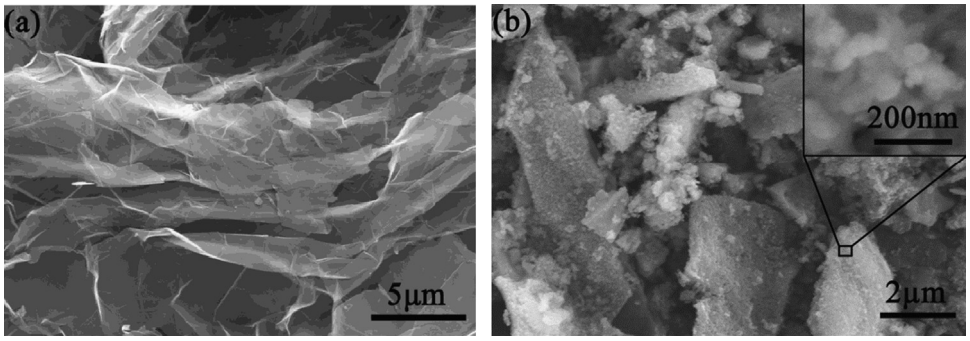

Fig. 1. FESEM images of (a) the pristine GNPs and (b) 1.5 wt% GNPs dispersed in BCP nanopowders.

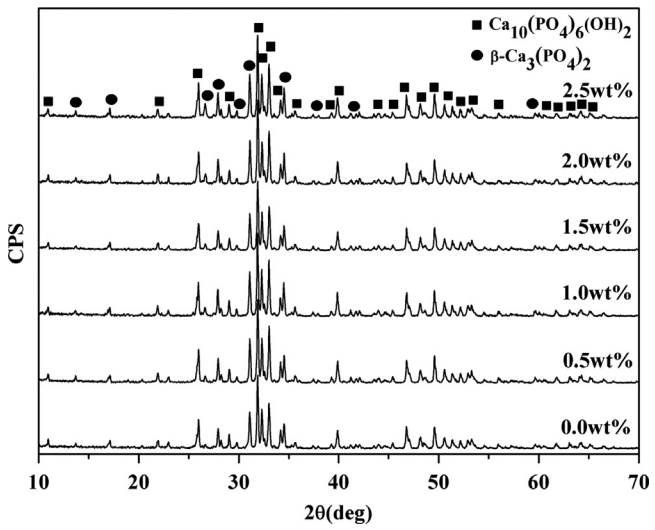

Fig. 2. XRD patterns of GNPs/BCP composites.

have high crystallinity after HP. The patterns are the same, which illustrates that the incorporations of GNPs have no effect on the stability of HA and β-TCP. GNPs are difficult to detect by XRD due to their small content, whereas their presence can be confirmed by FESEM and HRTEM images.

3.3. Sintered bulks

The sintered monolithic BCP and GNPs/BCP composites own high relative density as shown in Table 1. The addition of GNPs has little influence on the density of the composite; the content of GNPs increases and the relative density of the composite decreases slightly.

The polished and thermally etched surfaces of monolithic BCP and GNPs/BCP composites are compared in Fig. 3. The mean grain size is summarized in Table 1. The composites with different amounts of GNPs have almost the same grain size, approximately 1 μm. HA and β-TCP grains cannot be distinguished due to the similar size and shape in the FESEM images. As the FESEM images displayed, it is proved that GNPs have no apparent effect on grain size. The length and width of GNPs are about 0.5–20 μm, which is much larger than the grain size of BCP, therefore it cannot play a role of refining grains. This is much different from CNTs, which usually have greater effect on grain size through grain pinning [25].

Table 1
Relative density and grain size of the composites.

GNPs (wt%)	Relative density (%)	Mean grain size (μm)
0	98.54	1.04
0.5	98.38	1.00
1.0	98.24	1.15
1.5	98.11	1.21
2.0	97.43	1.00
2.5	96.74	1.07

3.4. Mechanical properties

The mechanical properties of GNPs/BCP composites were measured along two directions: parallel (designated by ‖) and perpendicular (⊥) to the HP direction, and the results are summarized in Table 2.

The direction parallel to the HP is the common test direction. In this direction, it is obvious that bending strength and fracture toughness are dependent upon the amount of GNPs greatly. The composite containing 1.5 wt% GNPs exhibits the maximum bending strength and fracture toughness of 151.82 MPa and 1.74 MPa $m^{1/2}$, about 55% and 76% higher than those of pure BCP, respectively. The measurement result for fracture toughness is influenced by the notch width and radius. In this experiment, comparatively high toughness values could be achieved due to the incision passivation. However, pure BCP and composites were tested using the same methods and conditions; at least, the values can prove that the GNPs are conducive to the improvement of fracture toughness. It can also be seen from the table that the addition of GNPs influences microhardness of the composites little; microhardness declines slightly with increase of GNPs.

In the direction perpendicular to the HP direction, a slight decrease in mechanical properties except fracture toughness is presented upon addition of 1.5 wt% GNPs. Compared with the values tested on the other direction, it is clear that monolithic BCP has similar mechanical properties, while the composite has poor mechanical properties. Intriguingly, the addition of GNPs leads to anisotropic mechanical properties, which is not reported previously. As we all know, the mechanical properties of bone are

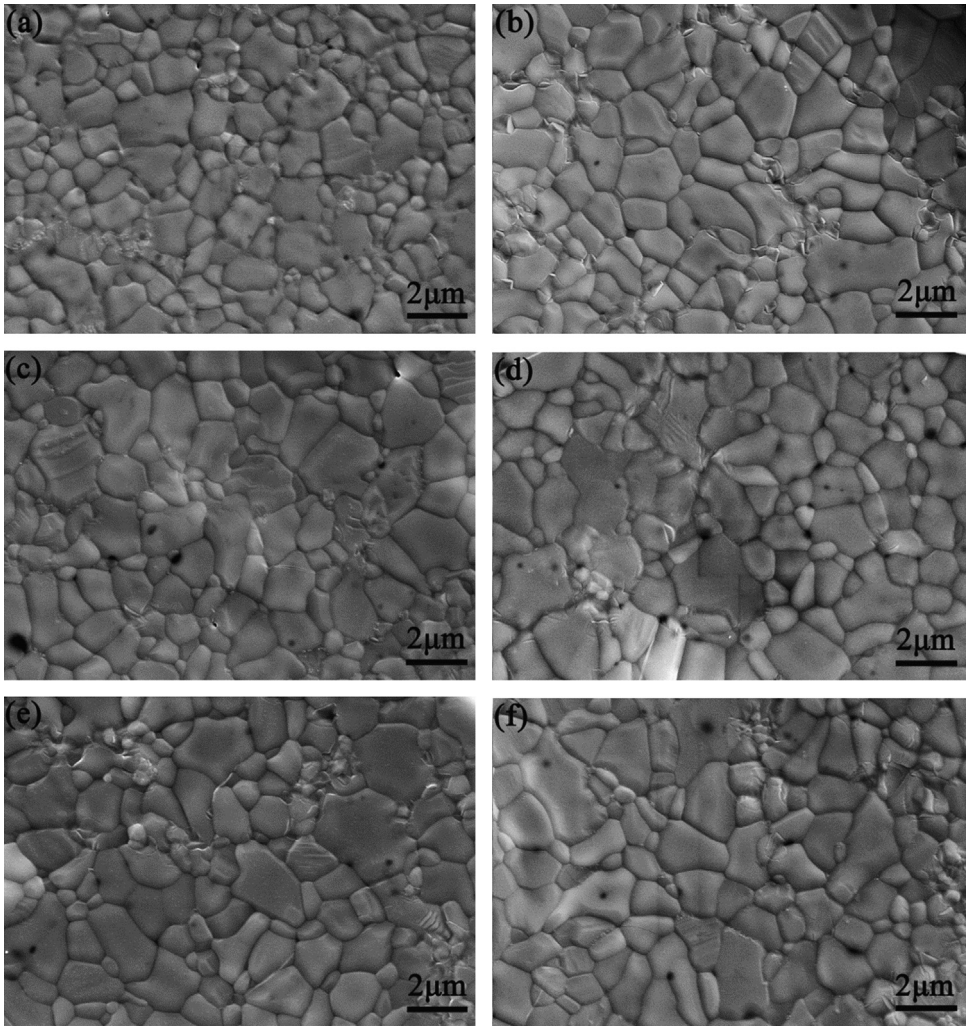

Fig. 3. FESEM images of thermally etched surfaces for (a) monolithic BCP, and the composites containing (b) 0.5 wt%, (c) 1.0 wt%, (d) 1.5 wt%, (e) 2.0 wt%, and (f) 2.5 wt% GNPs.

Table 2
Mechanical properties of GNPs/BCP composites.

GNPs (wt%)	Test direction	Bending strength σ_f (MPa)	Fracture toughness K_{IC} (MPa $m^{1/2}$)	Microhardness H (GPa)
0	∥	98.21±8.19	0.99±0.07	6.68±0.16
0.5	∥	121.43±7.06	1.38±0.03	6.41±0.22
1.0	∥	134.87±7.34	1.52±0.10	6.31±0.13
1.5	∥	151.82±7.03	1.74±0.07	6.18±0.09
2.0	∥	121.22±5.06	1.72±0.07	6.05±0.18
2.5	∥	117.79±4.43	1.69±0.03	5.81±0.23
0	⊥	84.99±3.78	0.94±0.10	6.63±0.13
1.5	⊥	68.86±6.94	1.38±0.09	6.09±0.12

also anisotropic. As compared with the typical mechanical properties of bone, GNPs/BCP composite has equivalent mechanical properties in both directions.

3.5. Microstructure

Fig. 4 shows FESEM images of fracture surfaces of the composites tested in the direction parallel to the HP direction. From the FESEM image of pure BCP in Fig. 4a, the fracture mode is almost trans-granular fracture. Fig. 4b–g shows the fracture surface of 1.5 wt% GNPs/BCP composite. From Fig. 4b, it can be observed that GNPs dispersed uniformly in the matrix, with the length and width up to several micrometers. The fracture mode is trans-granular fracture, similar to that of pure BCP. It is worth noting that the fracture surfaces on the sides of GNPs have different heights, as marked in Fig. 4b. It is demonstrated that GNPs can prevent the in-plane propagation of the crack, and the crack has to climb over GNPs to continue advancing. This means that GNPs can force crack to propagate in not just two but in three dimensions, similar to the experimental results of Walker et al. [12]. This can extend the crack propagation path, thereby improving the mechanical properties of the material. More details about GNPs are in high-magnification FESEM images (Fig. 4c–g). The GNPs locate at grain boundary, and follow the grain shape due to their high Young's modulus and great flexibility, as shown in Fig. 4c and d. The exposed GNPs, fractured parallel and perpendicular to the fracture surface and then pulled out from the matrix, are shown in Fig. 4c and d, respectively.

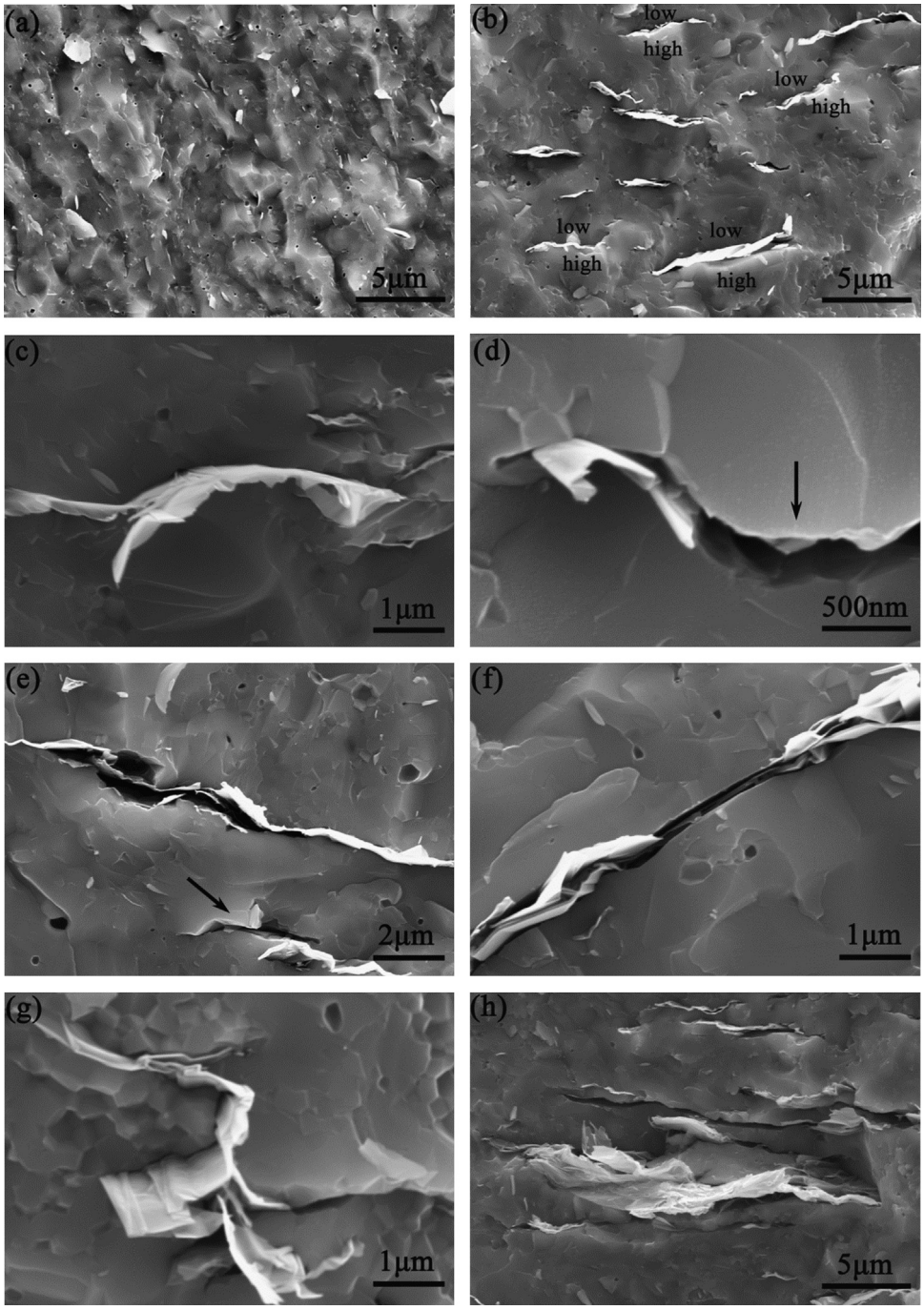

Fig. 4. FESEM images of the fracture surfaces of the composites tested in the direction parallel to the HP direction: (a) the trans-granular fracture mode of pure BCP, (b) the cracks climb over GNPs to propagate, (c)–(f) GNPs pulling out from the matrix, (g) GNPs wrap around the grains, and (h) the agglomeration of GNPs.

Fig. 4d and e can be observed the gaps left in the matrix after the pulling out of GNPs, as marked by black arrows. When a few GNPs overlap, the GNPs in the middle will be extracted during fracture (Fig. 4e and f). From Fig. 4c–g, it can be clearly seen that GNPs are pulled out of the fracture surface and the exposed GNPs are approximately 0.5–1 μm in length. The short pullout length proves that GNPs and BCP matrix have an appropriate bonding, which is of benefit to the improvement of mechanical properties. It is expected that the energy required to pull out a nanoplatelet is greater than that of a fiber or a nanotube owing to the larger contact area with the matrix. In addition, GNPs can also wrap around the grains (Fig. 4g), which inhibit the movement of grain boundary. The size of wrapped grain is small, about 400 nm, and its fracture mode has changed from trans-granular to inter-granular fracture, which will prolong the crack propagation path.

GNPs are prone to layered accumulation owing to their flat morphology and the interaction between the layers. Obviously,

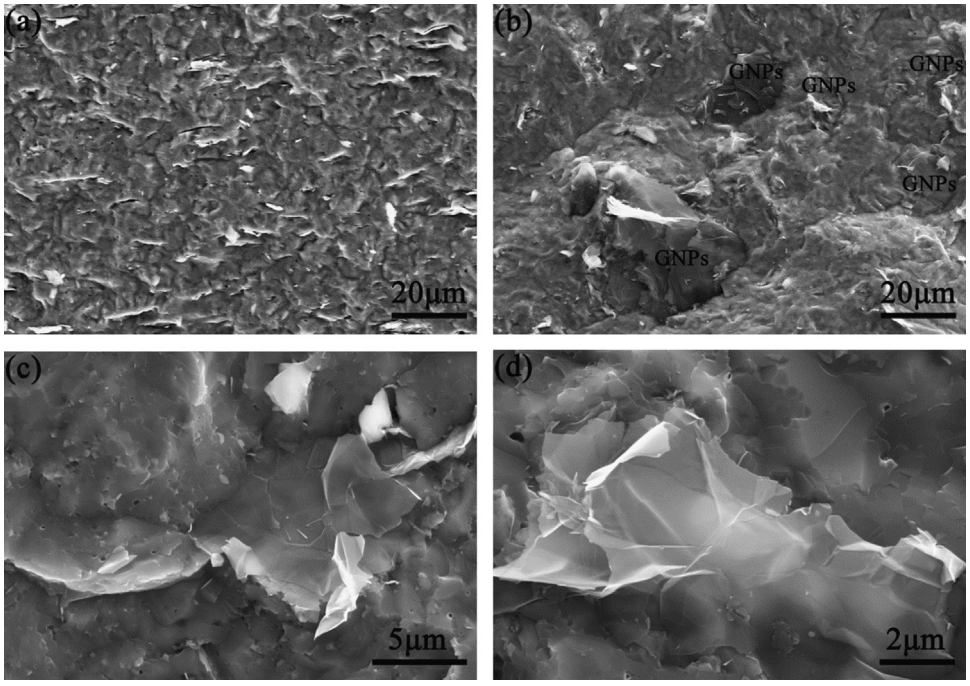

Fig. 5. FESEM images of the fracture surfaces of the composites tested in the direction (a) parallel and (b)–(d) perpendicular to the HP direction; (a) and (b) exhibit the different distributions of GNPs in two directions, and GNPs locate sloped (c) or parallel (d) to the fracture surface.

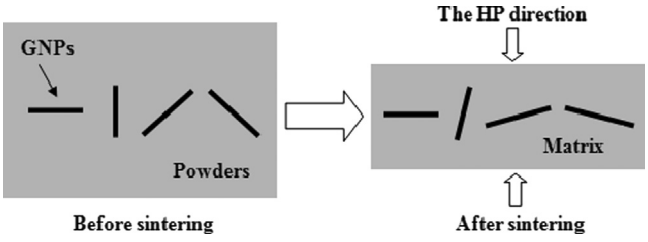

Fig. 6. Longitudinal section schematic of GNPs orientation.

agglomeration of GNPs exists in the sample containing 2.5 wt% GNPs (Fig. 4h). The agglomerations, like some defects in the sintered body, finally reduce the mechanical properties.

Fig. 5 shows FESEM images of the fracture surfaces tested in both directions. In comparison to Fig. 5a and b, it is clear that the distribution of GNPs in the two directions is completely different. During HP, GNPs orientate due to external pressure and flow of powders, that is, GNPs have the tendency to distribute perpendicular to the HP direction. The occurrence of this phenomenon is proved in the two images. In the direction perpendicular to the HP direction, GNPs locate sloped (Fig. 5c) or parallel (Fig. 5d) to the fracture surface. When crack encounters GNPs, it will propagate along the GNPs layers or the interface between GNPs and BCP matrix, so that the pullout of GNPs cannot be achieved, limiting the toughening effect of GNPs. The orientation distribution of GNPs results in anisotropy mechanical properties of the composites. The longitudinal section schematic of the composites is in Fig. 6, displaying the orientation of GNPs during sintering.

3.6. Interface

HRTEM examination was performed to obtain detailed information about microstructures. From Fig. 7a, it can be seen that GNPs are located on the grain boundaries bending and following the shape of grain, and the grain size is about 0.5–1 μm, which is similar to the observation in FESEM images. A single GNP with thickness of 5 nm is shown in Fig. 7b, which can be distinguished easily through its characteristic lattice. GNPs are extremely thin, but easy to agglomerate. Overlapped GNPs with thickness of about 20 nm are located between two grains (Fig. 7c), and the lattices of grains and GNPs can be seen clearly. Furthermore, the tight bonding between GNPs and matrix is clearly displayed in Fig. 7d, and no obvious diffusion layer is observed at the interface. The tight bonding is beneficial to transferring load between GNPs and the matrix and to forming bridging, finally leading to the improved mechanical properties.

3.7. Toughening mechanism

Fig. 8 shows the indentation-induced crack propagation on the polished surface of GNPs/BCP composite. Crack deflection, crack branching and interface debonding are observed clearly from Fig. 8a. During crack propagation, the stress field near crack tip is disturbed due to the presence of GNPs, thus crack changes the propagation direction and advances along the interface of GNPs and matrix, resulting in crack deflection and branching. Meanwhile, interface debonding occurs during crack advancement along the interface. In this process, the crack propagation path is extended and the fracture surface

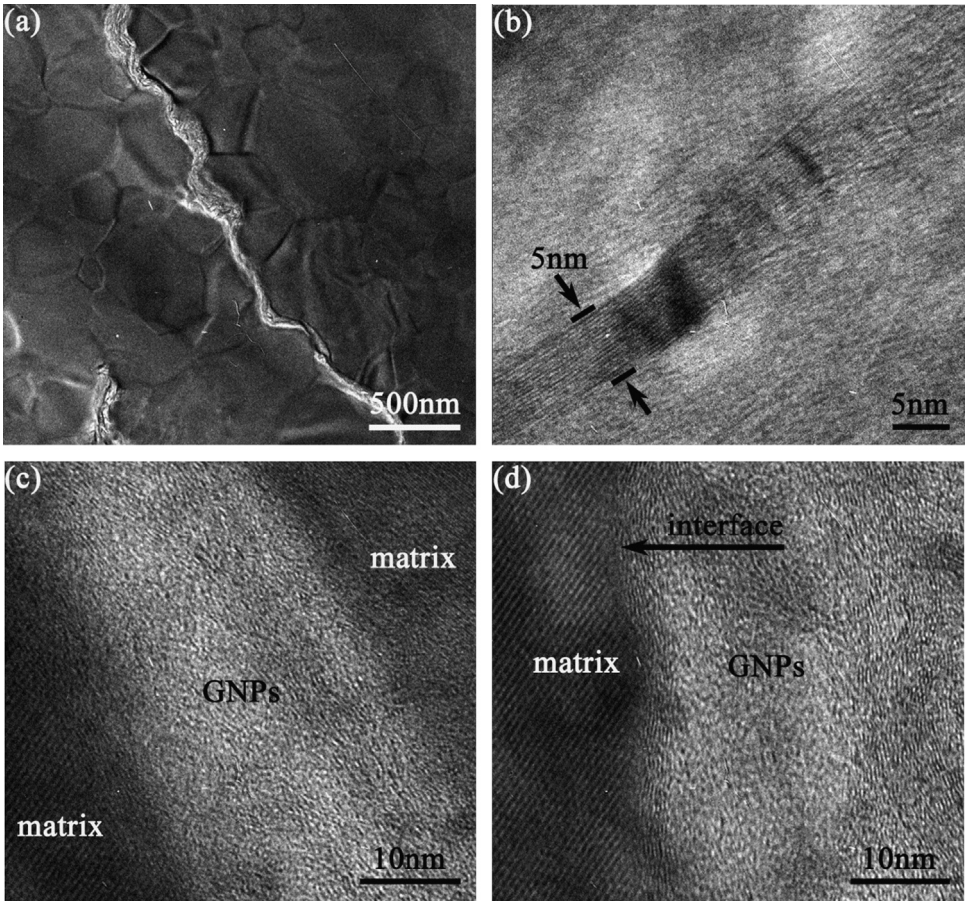

Fig. 7. HRTEM images of 1.5 wt% GNPs/BCP composite: (a) GNPs locate at grain boundary, (b) a single GNP with thickness of 5 nm, (c) overlapped GNPs locate between two grains, and (d) the interface of GNPs and matrix.

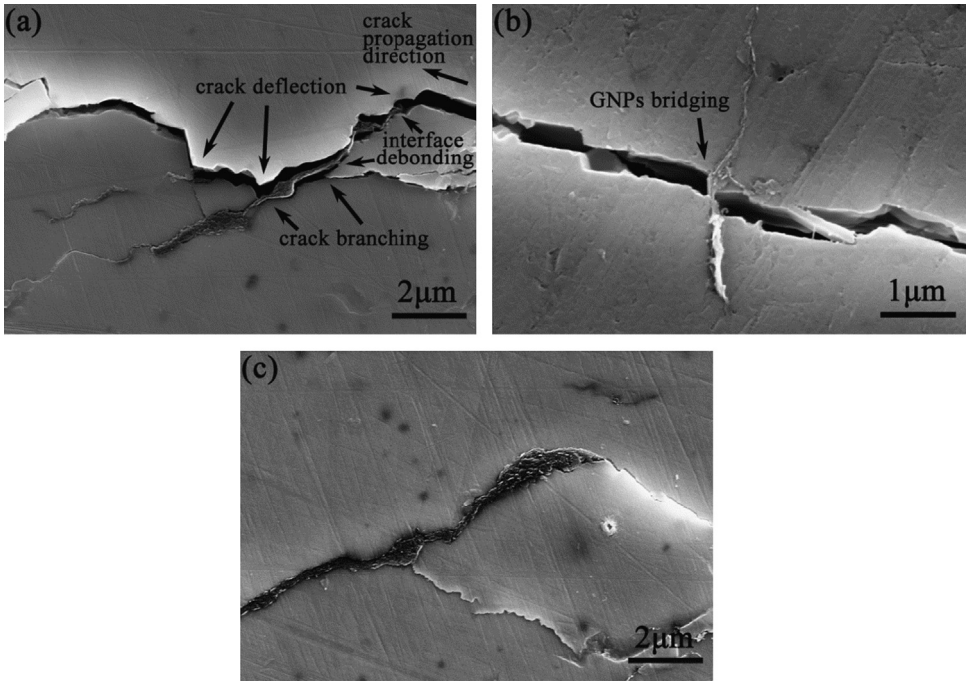

Fig. 8. Toughening mechanisms in GNPs/BCP composites: (a) crack deflection, crack branching and interface debonding, (b) GNPs bridging, and (c) cracks stopped at GNPs.

area increases, which will dissipate the energy of crack propagation, thereby improving the mechanical properties of the composite. Fig. 8b exhibits the occurrence of GNPs bridging, which is the typical toughening mechanism in the composite. As external force increases and crack propagates further, GNPs emerge gradually, and then fracture or get pulled out as displayed in Fig. 4c–g, which will consume the energy of crack propagation. In addition, GNPs can also force crack to propagate in three dimensions as observed from Fig. 4b. If driving force of crack propagation is not large enough, crack will be stopped at the GNPs, as shown in Fig. 8c.

4. Conclusions

To summarize, GNPs toughened BCP composite has been successfully fabricated through HP, and the mechanical properties of the composite parallel to the HP direction were greatly improved. GNPs tended to distribute perpendicular to the HP direction due to external pressure and flow of powders. The orientation distribution of GNPs resulted in anisotropic mechanical properties of the composites. Parallel to the HP direction, the composite containing 1.5 wt% GNPs exhibited the maximun bending strength and fracture toughness of 151.82 MPa and 1.74 MPa $m^{1/2}$, about 55% and 76% higher than those of monolithic BCP, respectively. During the composite fracturing, crack deflection, crack branching, bridging, pullout and fracture of GNPs happened. In particular, GNPs can force crack to propagate not only in two but also in three dimensions. These were dominantly responsible for the increase in mechanical properties. Consequently, GNPs may be an effective additive for toughening ceramics and other materials, and GNPs/BCP composite may be promising bone substitute materials.

Acknowlegment

This work was financially supported by National Natural Science Foundation of People's Republic of China (No. 81171463).

References

[1] A.K. Geim, K.S. Novoselov, The rise of graphene, Nature Materials 6 (2007) 183–191.
[2] Y. Zhu, S. Murali, W. Cai, X. Li, J.W. Suk, J.R. Potts, R.S. Ruoff, Graphene and graphene oxide: synthesis, properties, and applications, Advanced Materials 22 (2010) 3906–3924.
[3] C. Lee, X. Wei, J.W. Kysar, J. Hone, Measurement of the elastic properties and intrinsic strength of monolayer graphene, Science 321 (2008) 385–388.
[4] M. Poot, H.S.J. van der Zant, Nanomechanical properties of few-layer graphene membranes, Applied Physics Letters 92 (2008) 063111-3.
[5] F. Liu, P. Ming, J. Li, Ab initio calculation of ideal strength and phonon instability of graphene under tension, Physical Review B 76 (2007) 064120-7.
[6] K.S. Novoselov, A.K. Geim, S.V. Morozov, D. Jiang, Y. Zhang, S.V. Dubonos, I.V. Grigorieva, A.A. Firsov, Electric field effect in atomically thin carbon films, Science 306 (2004) 666–669.
[7] A.A. Balandin, S. Ghosh, W. Bao, I. Calizo, D. Teweldebrhan, F. Miao, C.N. Lau, Superior thermal conductivity of single-layer graphene, Nano Letters 8 (2008) 902–907.
[8] L. Chen, Y. Hernandez, X. Feng, K. Müllen, From nanograhpene and graphene nanoribbons to graphene sheets: chemical synthesis, Angewandte Chemie International Edition 51 (2012) 7640–7654.
[9] X. Huang, X. Qi, F. Boey, H. Zhang, Graphene-based composites, Chemical Society Reviews 41 (2012) 666–686.
[10] K. Wang, Y. Wang, Z. Fan, J. Yan, T. Wei, Preparation of graphene nanosheet/alumina composites by spark plasma sintering, Materials Research Bulletin 46 (2011) 315–318.
[11] J. Liu, H. Yan, M.J. Reece, K. Jiang, Toughening of zirconia/alumina composites by the addition of graphene platelets, Journal of the European Ceramic Society 32 (2012) 4185–4193.
[12] L.S. Walker, V.R. Marotto, M.A. Rafiee, N. Koratkar, E.L. Corral, Toughening in graphene ceramic composites, ACS Nano 5 (2011) 3182–3190.
[13] J. Dusza, J. Morgiel, A. Duszová, L. Kvetková, M. Nosko, P. Kun, C. Balázsi, Microstructure and fracture toughness of Si_3N_4+graphene platelet composites, Journal of the European Ceramic Society 32 (2012) 3389–3397.
[14] L. Kvetková, A. Duszová, P. Hvizdoš, J. Dusza, P. Kun, C. Balázsi, Fracture toughness and toughening mechanisms in graphene platelet reinforced Si_3N_4 composites, Scripta Materialia 66 (2012) 793–796.
[15] P. Kun, O. Tapasztó, F. Wéber, C. Balázsi, Determination of structural and mechanical properties of multilayer graphene added silicon nitride-based composites, Ceramics International 38 (2012) 211–216.
[16] J. Zhu, H.M. Wong, K.W.K. Yeung, S.C. Tjong, Spark plasma sintered hydroxyapatite/graphite nanosheet and hydroxyapatite/multiwalled carbon nanotube composites: mechanical and in vitro cellular properties, Advanced Engineering Materials 13 (2011) 336–341.
[17] Y. Fan, L. Wang, J. Li, J. Li, S. Sun, F. Chen, L. Chen, W. Jiang, Preparation and electrical properties of graphene nanosheet/Al_2O_3 composites, Carbon 48 (2010) 1743–1749.
[18] C. Ramirez, F.M. Figueiredo, P. Miranzo, P. Poza, M.I. Osendi, Graphene naoplatelet/silicon nitride composites with high electrical conductivity, Carbon 50 (2012) 3607–3615.
[19] P. Miranzo, E. García, C. Ramírez, J. González-Julián, M. Belmonte, M.I. Osendi, Anisotropic thermal conductivity of silicon nitride ceramics containing carbon nanostructures, Journal of the European Ceramic Society 32 (2012) 1847–1854.
[20] C. Ramirez, L. Garzón, P. Miranzo, M.I. Osendi, C. Ocal, Electrical conductivity maps in graphene nanoplatelet/silicon nitride composites using conducting scanning force microscopy, Carbon 49 (2011) 3873–3880.
[21] R.Z. Legeros, S. Lin, R. Rohanizadeh, D. Mijares, J.P. Legeros, Biphasic calcium phosphate bioceramics: preparation, properties and applications, Journal of Materials Science—Materials in Medicine 14 (2003) 201–209.
[22] E. Buache, F. Velard, E. Bauden, C. Guillaume, E. Jallot, J.M. Nedelec, D. Laurent-Maquin, P. Laquerriere, Effect of strontium-substituted biphasic calcium phosphate on inflammatory mediators production by human monocytes, Acta Biomaterialia 8 (2012) 3113–3119.
[23] E. Ghomash Pasand, A. Nemati, M. Solati-Hashjin, K. Arzani, A. Farzadi, Microwave assisted synthesis & properties of nano HA–TCP biphasic calcium phosphate, International Journal of Minerals, Metallurgy and Materials 19 (2012) 441–445.
[24] J.H. Lee, D.W. Shin, V.G. Makotchenko, A.S. Nazarov, V.E. Fedorov, J.H. Yoo, S.M. Yu, J.Y. Choi, J.M. Kim, J.B. Yoo, The superior dispersion of easily soluble graphite, Small 6 (2010) 58–62.
[25] D. Lahiri, V. Singh, A.K. Keshri, S. Seal, A. Agarwal, Carbon nanotube toughened hydroxyapatite by spark plasma sintering: microstructural evolution and multiscale tribological properties, Carbon 48 (2010) 3103–3120.